


# Compound-induced transparency in three-cavity coupled structure

Hao-Ye Qin(秦昊烨), Yi-Heng Yin(尹贻恒), and Ming Ding(丁铭)

**Citation:**Chin. Phys. B, 2020, 29 (**12**): 124208. DOI: 10.1088/1674-1056/abab7e
Journal homepage: http://cpb.iphy.ac.cn; http://iopscience.iop.org/cpb

**What follows is a list of articles you may be interested in**

---

## Eigenvalue spectrum analysis for temporal signals of Kerr optical frequency combs based on nonlinear Fourier transform

Jia Wang(王佳), Ai-Guo Sheng(盛爱国), Xin Huang(黄鑫), Rong-Yu Li(李荣玉), Guang-Qiang He(何广强)
Chin. Phys. B, 2020, 29 (**3**): 034207. DOI: 10.1088/1674-1056/ab683a

## Cavity optomechanics: Manipulating photons and phonons towards the single-photon strong coupling

Yu-long Liu(刘玉龙), Chong Wang(王冲), Jing Zhang(张靖), Yu-xi Liu(刘玉玺)
Chin. Phys. B, 2018, 27 (**2**): 024204. DOI: 10.1088/1674-1056/27/2/024204

## Theoretical analysis of the electromagnetic field inside an anomalous-dispersion microresonator under synthetical pump

Xin Xu(徐昕), Xiaohong Hu(胡晓鸿), Ye Feng(冯野), Yuanshan Liu(刘元山), Wei Zhang(张伟), Zhi Yang(杨直), Wei Zhao(赵卫), Yishan Wang(王屹山)
Chin. Phys. B, 2016, 25 (**3**): 034208. DOI: 10.1088/1674-1056/25/3/034208

## A quartz-enhanced photoacoustic spectroscopy sensor for measurement of water vapor concentration in the air

Gong Ping, Xie Liang, Qi Xiao-Qiong, Wang Rui, Wang Hui, Chang Ming-Chao, Yang Hui-Xia, Sun Fei, Li Guan-Peng
Chin. Phys. B, 2015, 24 (**1**): 014206. DOI: 10.1088/1674-1056/24/1/014206

## Electromagnetically induced transparency in a three-mode optomechanical system

Yan Xiao-Bo, Gu Kai-Hui, Fu Chang-Bao, Cui Cui-Li, Wu Jin-Hui
Chin. Phys. B, 2014, 23 (**11**): 114201. DOI: 10.1088/1674-1056/23/11/114201

---

# Compound-induced transparency in three-cavity coupled structure*

Hao-Ye Qin(秦昊烨)[1], Yi-Heng Yin(尹贻恒)[1], and Ming Ding(丁铭)[1,2,†]

[1] School of Instrumentation and Opto-Electronics Engineering, Beihang University, Beijing 100191, China
[2] Research Institute of Frontier Science, Beihang University, Beijing 100191, China

(Received 22 May 2020; revised manuscript received 23 June 2020; accepted manuscript online 1 August 2020)

We propose a three-cavity coupled cavity optomechanical (COM) structure with tunable system parameters and theoretically investigate the probe-light transmission rate. Numerical calculation of the system's spectra demonstrates distinctive compound-induced transparency (CIT) characteristics, including multiple transparency windows and sideband dips, which can be explained by a coupling between optomechanically-induced transparency (OMIT) and electromagnetically-induced transparency. The effects of optical loss (gain) in the cavity, number and topology of active cavity, tunneling ratio, and pump laser power on the CIT spectrum are evaluated and analyzed. Moreover, the optical group delay of CIT is highly controllable and fast–slow light inter-transition can be achieved. The proposed structure makes possible the advantageous tuning freedom and provides a potential platform for controlling light propagation and fast–slow light switching.

**Keywords:** microresonator, cavity optomechanics, optomechanically-induced transparency, slow light, electromagnetically-induced transparency

**PACS:** 42.60.Da, 42.50.Gy **DOI:** 10.1088/1674-1056/abab7e

## 1. Introduction

Electromagnetically-induced transparency (EIT) is an interesting and unexpected phenomenon resulting from quantum coherence. The most direct way to achieve the EIT effect is to employ coupled cavities, *i.e.*, a microresonator system with two coupled optical whispering gallery modes (WGMs).[1] The progress of fabrication techniques makes it possible to produce high-$Q$-factor mechanical oscillators and subsequently the optomechanical systems. As a counterpart and analogy to EIT, optomechanically-induced transparency (OMIT)[2] has been proposed recently and could be generated through cavity optomechanical (COM) interaction.[3,4] The fundamental physics of OMIT lies in the three-level $\Lambda$-type atomic system[4–7] and it allows writing and reading out the optical information as a long-lived mechanical excitation. The OMIT has been demonstrated experimentally to make it possible to control the light propagation by employing nano- and micro-mechanical structures,[6–9] in both optical and microwave regimes.[10,11]

Recent studies of COM have focused on the modification of the single-cavity structures by adding another cavity and thus introducing the compound COM (coupled two cavities),[8,9,12] which opens up a promising route to implementing devices such as phonon lasers,[13,14] stationary (photonic) qubits,[15,16] and coherent optical wavelength converters.[17,18] As a combination of coupled-cavity-induced EIT and OMIT, double OMIT has been shown in a compound COM system.[9] Besides, other superior features presented by compound COM have been exploited to allow for enhanced nonlinearities[19] and optically induced energy transfer.[20] Inspired by parity–time-symmetric structure with passive–active–coupled cavities,[21] in 2015 an inverted OMIT spectrum was proposed and identified in a similar compound COM structure with a tunable gain-to-loss ratio, featuring a sideband-reversed non-amplifying transparency.[8] This structure of active–passive–coupled cavity has also been revealed to demonstrate the active higher-order nonlinear OMIT effects, which can achieve the optical delay or advance on a scale of hundreds of microseconds.[12] However, there still exist some new physical phenomena and promising applications for all-optics devices based on the extension of this COM structure.

In this paper, we propose a novel active COM structure by incorporating a third cavity to the previous two-cavity compound COM system, which demonstrates a novel compound-induced transparency (CIT) spectrum and large degree of tuning freedom. Unlike the two-cavity condition (active-passive coupled) in Ref. [8], this three-cavity structure results in interesting multiple transparency windows and sidebands dips (peaks), which can be understood as a coupling between OMIT and EIT. Theoretical model of probe-light transmission rate in this structure is derived and its transmission spectrum is numerically calculated to demonstrate the features of interplay between OMIT and EIT. The optical group delay of the system is greatly modified and controllable, which enables the switch from fast light to slow light, and *vice versa*.

## 2. Theoretical model

### 2.1. Schematic diagram of the proposed compound system

As shown in the schematic diagram, the compound system is composed of three coupled microresonators, which involve three optical modes ($a_i$) and one mechanical mode ($b$)

*Project supported by the National Natural Science Foundation of China (Grant No. 61575014).
†Corresponding author. E-mail: mingding@buaa.edu.cn
© 2020 Chinese Physical Society and IOP Publishing Ltd

with frequency $\omega_m$ and an effective mass $m$. We regard the first resonator as a passive optomechanical resonator with an optical loss rate of $\gamma_1$, and the second and third resonators can either be active or passive, with optical loss (gain) rate denoted by $\gamma_2$, $\gamma_3 > 0$ ($< 0$), respectively. For example, the proportion $\gamma_1 : \gamma_2 : \gamma_3 = 1 : -1 : 1$ refers to a passive–active–passive coupled optomechanical system and each resonator has the same absolute value of optical loss (gain) rate. And the coupling strengths $J_1$ and $J_2$ between the resonators can be tuned by adjusting the distance between them.

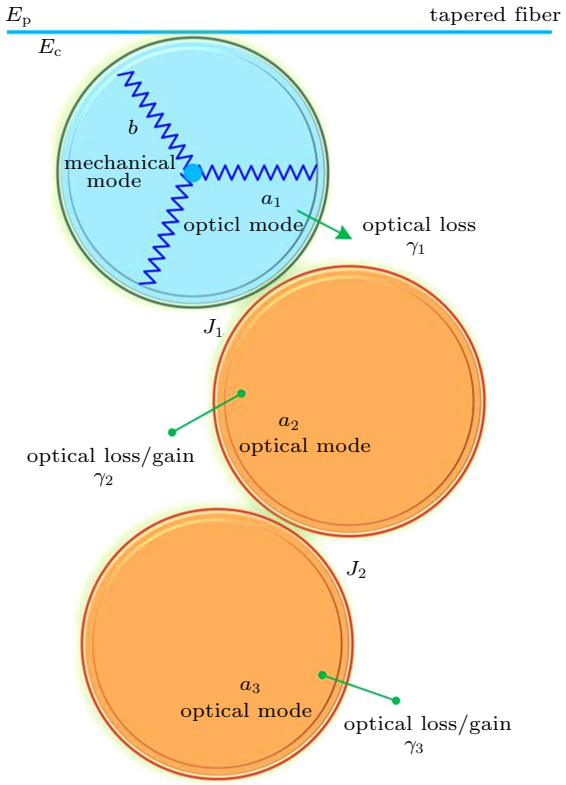



**Fig. 1.** Schematic diagram of compound COM structure containing three cavities with a mechanical mode ($b$) and three optical modes ($a_1$, $a_2$, and $a_3$). Gain (loss) ratio ($\gamma_i$), number of active cavities and intercavity tunneling rate ($J_i$) are tunable.

### 2.2. Deviation of transmission rate

To achieve CIT, both a strong pump laser with frequency $\omega_L$ and weak probe light with frequency $\omega_p$ are used through the tapered fiber and coupled to this compound system. The amplitudes of the pump and probe light are given as $E_L = \sqrt{2\gamma_1 P_L/\hbar\omega_L}$ and $E_p = \sqrt{2\gamma_1 P_{in}/\hbar\omega_p}$, where $P_L$ and $P_{in}$ denote the pump power and the probe power, respectively.

The Hamiltonian of this four-mode coupling compound system can be written as

$$\begin{aligned} H &= H_0 + H_{int} + H_{dr}, \\ H_0 &= \hbar\Delta_L(a_1^\dagger a_1 + a_2^\dagger a_2 + a_3^\dagger a_3) + \frac{p^2}{2m} + \frac{1}{2}m\omega_m^2 x^2, \\ H_{int} &= -\hbar J_1(a_1^\dagger a_2 + a_2^\dagger a_1) - \hbar J_2(a_2^\dagger a_3 + a_3^\dagger a_2) - \hbar g a_1^\dagger a_1 x, \\ H_{dr} &= \mathrm{i}\hbar(E_L a_1^\dagger - E_L a_1 + E_p a_1^\dagger \mathrm{e}^{-\mathrm{i}\xi t} - E_p a_1 \mathrm{e}^{\mathrm{i}\xi t}), \end{aligned} \tag{1}$$

where $a_1$, $a_2$, and $a_3$ denote the annihilation operators of the bosonic fields in the microresonators with resonance frequency $\omega_c$; $R$ is the radius; the optomechanical coupling rates fit with the relation of $g = \omega_c/R$. The pump–resonator, probe–resonator, and probe–pump frequency detunings are respectively expressed as $\Delta_L = \omega_c - \omega_L$, $\Delta_p = \omega_p - \omega_c$, $\xi = \omega_p - \omega_L$.

The Heisenberg equations of motion (EOM) of this compound system can be discribed as

$$\begin{aligned} \ddot{x} + \Gamma_m \dot{x} + \omega_m^2 x &= \frac{\hbar g}{m} a_1^+ a_1, \\ \dot{a}_1 &= (-\mathrm{i}\Delta_L + \mathrm{i}gx - \gamma_1)a_1 + \mathrm{i}J_1 a_2 + E_L + E_p \mathrm{e}^{-\mathrm{i}\xi t}, \\ \dot{a}_2 &= (-\mathrm{i}\Delta_L - \gamma_2)a_2 + \mathrm{i}J_1 a_1 + \mathrm{i}J_2 a_3, \\ \dot{a}_3 &= (-\mathrm{i}\Delta_L - \gamma_3)a_3 + \mathrm{i}J_2 a_2. \end{aligned} \tag{2}$$

Setting the derivative terms in the EOM to be zero, the resulting steady-state values of the dynamical variables are

$$\begin{aligned} x_s &= \frac{\hbar g}{m\omega_m^2}|a_{1,s}|^2, \quad a_{1,s} = \frac{-E_L\left[(-\mathrm{i}\Delta_L - \gamma_2)(\mathrm{i}\Delta_L + \gamma_1) - J_2^2\right]}{(-\mathrm{i}\Delta_L + \mathrm{i}gx_s - \gamma_1)\left[(-\mathrm{i}\Delta_L - \gamma_2)(\mathrm{i}\Delta_L + \gamma_3 - J_2^2) + J_1^2(\mathrm{i}\Delta_L + \gamma_3)\right] + J_1^2(\mathrm{i}\Delta_L + \gamma_3)}, \\ a_{2,s} &= \frac{1}{\mathrm{i}J_1}\left[-E_L - a_{1,s}(-\mathrm{i}\Delta_L + \mathrm{i}gx_s - \gamma_1)\right], \quad a_{3,s} = \frac{\mathrm{i}J_2 a_{2,s}}{\mathrm{i}\Delta_L + \gamma_3}. \end{aligned} \tag{3}$$

To further deal with the problem, we treat each operator as the sum of its steady-state value and a small fluctuation around that value, that is,

$$\begin{aligned} &a_1 = a_{1,s} + \delta a_1, \quad a_2 = a_{2,s} + \delta a_2, \\ &a_3 = a_{3,s} + \delta a_3, \quad x = x_s + \delta x. \end{aligned}$$

Then the expected values of the operators are expanded as follows:

$$\begin{pmatrix} \langle a_1 \rangle \\ \langle a_2 \rangle \\ \langle a_3 \rangle \\ \langle x \rangle \end{pmatrix} = \begin{pmatrix} a_{1,s} \\ a_{2,s} \\ a_{3,s} \\ x_s \end{pmatrix} + \begin{pmatrix} \delta a_{1+} \\ \delta a_{2+} \\ \delta a_{3+} \\ \delta x_+ \end{pmatrix} \mathrm{e}^{-\mathrm{i}\xi t} + \begin{pmatrix} \delta a_{1-} \\ \delta a_{2-} \\ \delta a_{3-} \\ \delta x_- \end{pmatrix} \mathrm{e}^{\mathrm{i}\xi t}. \tag{4}$$

Linearized EOM can be obtained by eliminating the

steady-state values and solved by using the ansatz

$$
\begin{aligned}
&(\omega_m^2-\xi^2-\mathrm{i}\xi\Gamma_m)\delta x_+ = \frac{g}{m}(a_{1,\mathrm{s}}^*\delta a_{1+}+a_{1,\mathrm{s}}\delta a_{1-}),\\
&(\omega_m^2-\xi^2+\mathrm{i}\xi\Gamma_m)\delta x_- = \frac{g}{m}(a_{1,\mathrm{s}}^*\delta a_{1-}+a_{1,\mathrm{s}}\delta a_{1+}),\\
&(\mathrm{i}\Delta_\mathrm{L}+\gamma_1-\mathrm{i}gx_\mathrm{s}-\mathrm{i}\xi)\delta a_{1+} = \mathrm{i}J_1\delta a_{2+}+\mathrm{i}ga_{1,\mathrm{s}}\delta x_+ + E_\mathrm{p},\\
&(\mathrm{i}\Delta_\mathrm{L}+\gamma_1-\mathrm{i}gx_\mathrm{s}-\mathrm{i}\xi)\delta a_{1-} = \mathrm{i}J_1\delta a_{2-}+\mathrm{i}ga_{1,\mathrm{s}}\delta x_-,\\
&(\mathrm{i}\Delta_\mathrm{L}+\gamma_2-\mathrm{i}\xi)\delta a_{2+} = \mathrm{i}J_1\delta a_{1+}+\mathrm{i}J_2\delta a_{3+},\\
&(\mathrm{i}\Delta_\mathrm{L}+\gamma_2+\mathrm{i}\xi)\delta a_{2-} = \mathrm{i}J_1\delta a_{1-}+\mathrm{i}J_2\delta a_{3-},\\
&(\mathrm{i}\Delta_\mathrm{L}+\gamma_3-\mathrm{i}\xi)\delta a_{3+} = \mathrm{i}J_2\delta a_{2+},\\
&(\mathrm{i}\Delta_\mathrm{L}+\gamma_3+\mathrm{i}\xi)\delta a_{3-} = \mathrm{i}J_2\delta a_{2-}.
\end{aligned}
\tag{5}
$$

Since the value of interest is only $\delta a_{1+}$, solving these algebraic equations we have the following results:

$$
\delta a_{1+} = \frac{(E_\mathrm{p}/\mathrm{i}g)(\omega_m^2-\xi^2-\mathrm{i}\xi\Gamma_m)}{(\omega_m^2-\xi^2-\mathrm{i}\xi\Gamma_m)K_1-\dfrac{g}{m}|a_{1,\mathrm{s}}|^2-\dfrac{g^2}{m^2}\dfrac{|a_{1,\mathrm{s}}|^4}{(\omega_m^2-\xi^2-\mathrm{i}\xi\Gamma_m)K_2-\dfrac{g}{m}|a_{1,\mathrm{s}}|^2}} \tag{6}
$$

with

$$
\begin{aligned}
K_1 &= \frac{1}{\mathrm{i}g}\left(\mathrm{i}\Delta_\mathrm{L}+\gamma_1-\mathrm{i}gx_\mathrm{s}-\mathrm{i}\xi+\frac{J_1^2}{\mathrm{i}\Delta_\mathrm{L}+\gamma_2-\mathrm{i}\xi+\dfrac{J_2^2}{\mathrm{i}\Delta_\mathrm{L}+\gamma_3-\mathrm{i}\xi}}\right),\\
K_2 &= \frac{1}{-\mathrm{i}g}\left(-\mathrm{i}\Delta_\mathrm{L}+\gamma_1+\mathrm{i}gx_\mathrm{s}-\mathrm{i}\xi+\frac{J_1^2}{-\mathrm{i}\Delta_\mathrm{L}+\gamma_2-\mathrm{i}\xi+\dfrac{J_2^2}{-\mathrm{i}\Delta_\mathrm{L}+\gamma_3-\mathrm{i}\xi}}\right).
\end{aligned}
\tag{7}
$$

To numerically calculate the transmission spectrum for probe light, we employ the standard input–output relation $a_1^\mathrm{out} = a_1^\mathrm{in} - \sqrt{\gamma_1}a_1$ and generate the output probe field value, where $a_1^\mathrm{in}$ and $a_1^\mathrm{out}$ are the input and output field operators. Then the optical transmission rate (the squared amplitude of the ratio of the output field amplitude to the input field amplitude) reads

$$
\left|t_\mathrm{p}(\omega_\mathrm{p})\right|^2 = \left|\frac{a_1^\mathrm{out}}{a_1^\mathrm{in}}\right|^2 = \left|1-\frac{\gamma_1}{E_\mathrm{p}}\delta a_{1+}(\omega_\mathrm{p})\right|^2. \tag{8}
$$

For the better demonstrating the probe light transmission features, several spectra are plotted for the commonly available conditions,[8] *i.e.* experimentally-accessible parameters $R = 34.5$ μm, $\omega_\mathrm{c} = 1.93\times10^5$ GHz, $\omega_m = 2\pi\times23.4$ MHz, $m = 5\times10^{-11}$ kg, $\gamma_1 = 6.43$ MHz, $\Gamma_m = 2.4\times10^5$ Hz, $\Delta_\mathrm{L} = \omega_\mathrm{c}-\omega_\mathrm{L} = \omega_m$, and $\Delta_\mathrm{p} \equiv \omega_\mathrm{p}-\omega_\mathrm{c}$.

The transmission spectrum of the COM system can be changed by adjusting the number of optical capacities and the value of gain and loss of optical cavity. The optical tunneling rate between two resonators and the pump light power will also induce the compound transparency spectrum to change.

## 3. Results

Adding the third cavity makes the system consist of two coupled subsystems, an optomechanical system (first-second cavity coupling) exhibiting OMIT feature, and an optical coupled-cavity system (second–third cavity coupling) exhibiting EIT feature. As is illustrated from the transmission rate in Eq. (8), the compound-induced transparency spectrum is dependent on several tunable system parameters. Hereby, in this section the numerically calculated spectra and effects of different parameters are presented and evaluated.

### 3.1. Effect of $\gamma_2$ and $\gamma_3$ on CIT spectrum

In the first place, the optical gain rate $\gamma_2$ and loss rate $\gamma_3$ in the second and third cavity are investigated for their effects on the probe transmission spectrum. By introducing optical gain into the second cavity, this compound COM system is first preset to be passive–active–passive. A typical condition of $J_1 = \gamma_1$, $J_1/J_2 = 1$ and $P_\mathrm{L} = 1$ μW is selected, and figure 2 demonstrates the relevant calculated transmission spectra with different values of $\gamma_2$ and $\gamma_3$. The detailed gain/loss values are added along the lineshape in individual figure. For comparison, the red solid line represents $\gamma_2 < 0$ (the second resonator is active, inducing optical gain) and the blue dashed line represents $\gamma_2 > 0$ (the second resonator is passive, inducing optical loss).

These CIT spectra show an interesting feature quantified by four dips and three transparency windows, including one at the zero-detuning position and two sideband peaks. Intuitively, the distinctive CIT spectra can be explained as originating from collective effects of inverted EIT and OMIT. An active second cavity serves as a middleman, because it can not only couple with the first optomechanical cavity to result in an inverted OMIT, but interact with the third optical cavity to form an inverted EIT.[22] Therefore, in the transmission spectrum, the on-resonance peak reveals the feature of OMIT, and

two sideband peaks demonstrate the presence of EIT.

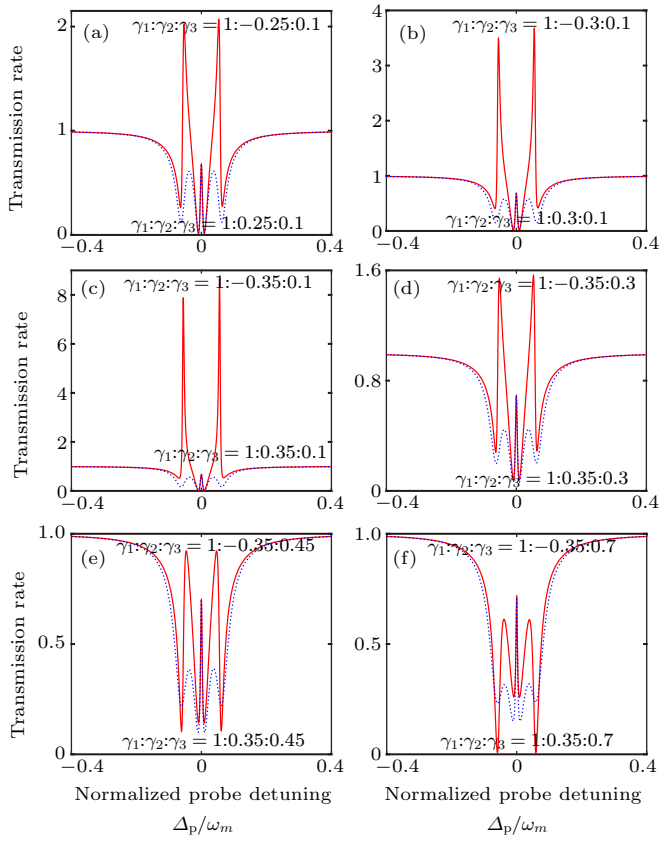



**Fig. 2.** Transmission spectra of probe light in active–passive–active–coupled system, with red solid line for $\gamma_2 < 0$ case and blue dashed line for $\gamma_2 > 0$ case. Detailed optical loss–gain ratios are denoted in individual figures, and relevant parameters are selected as $J_1 = \gamma_1$, $J_1/J_2 = 1$, and $P_L = 1$ μW.

Increasing the optical gain (reducing $\gamma_2$) into the second cavity contributes to enhanced sideband peaks (see Figs. 2(a)–2(c)) while increasing the optical loss in the third cavity (increasing $\gamma_3$) will result in shallower sideband peaks, whose heights are able to be tuned from larger to lower value than the height of on-resonance window (see Figs. 2(c)–2(f)). A close inspection of the three-passive-cavity case, the on-resonance transparency window has the same lineshape as that of the passive–active–passive case. Also, by tuning the gain rate and the loss rate, the two farthest dips from on-resonance window can range from the shallower (*i.e.*, Fig. 2(d)) to the deeper (*i.e.*, Fig. 2(f)) than secnarios of the three-passive-cavity case. Since the two sideband peaks reflect the EIT feature, this phenomenon corresponds to the increasing of optical loss to a value of an active–passive–coupled EIT system, which generates suppressed sidebands. Within these tuning ranges, the height of the on-resonance peak (OMIT feature) remains relatively stable.

### 3.2. Effect of number of active resonators on CIT spectrum

A distinctive feature of the proposed three-cavity structure is that both the number of active cavities and the passive–active-coupling topology are tunable. To achieve these, one can introduce optical gain into either the second or third cavity, or make them act as active cavities. Here two special cases are chosen, and their probe transmission spectra are numerically calculated.

Figure 3(a) shows the case of a structure including two active cavities, that is, a passive–active–active structure. In contrast with the passive–active–passive case, denoted by blue dashed line, introducing additional gain into the third cavity results in larger sideband transparency peaks, but other transmission features are identical. Figure 3(b) demonstrates the condition of passive–passive–active coupling, where the optical gain is present in the third cavity instead of the second one. This topological change results in broadened sideband transparency windows, whose lineshapes are delicately different from the former results. Examined from the peak maximum, sideband transparency windows in this case presents Romanesque (domical) profiles, while those in the passive–active–passive shows Gothic (spire-like) profiles.

These results clearly confirm the previous explanation that the EIT feature from coupling of the second and third cavity leads to the two sideband peaks, on which the optical loss (gain) rate of the third cavity mainly has an influence.

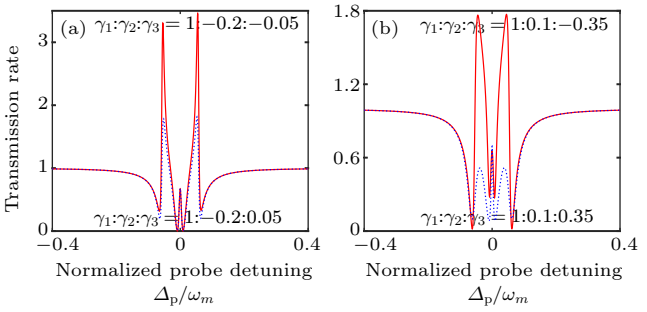



**Fig. 3.** Transmission rate changing with normalized probe signal detuning of probe light for (a) $\gamma_1 : \gamma_2 : \gamma_3 = 1 : -0.2 : -0.05$, and (b) $\gamma_1 : \gamma_2 : \gamma_3 = 1 : 0.1 : -0.35$ of probe light, with red solid line and blue dashed line showing condition of $\gamma_3 < 0$ and $\gamma_3 > 0$, respectively, and relevant parameters being selected as $J_1 = \gamma_1, J_1/J_2 = 1$, and $P_L = 1$ μW.

### 3.3. Effect of tunneling ratio ($J_1/J_2$) between two resonators on CIT spectrum

Here the ratio of the optical tunneling rate between two coupled cavities is defined as tunneling ratio, equal to $J_1/J_2$. A passive–active–passive structure with $\gamma_1 : \gamma_2 : \gamma_3 = 1 : -0.38 : 0.29$ is considered. Figure 4 shows four transmission spectra with different tunneling ratios, *i.e.*, 0.05, 0.5, 1.3, and 1.6. At $J_1/J_2 = 0.05$, the transmission demonstrates a downward on-resonance transparency window between two sideband peaks. This is because there is nearly no coupling between the second and third cavity (thus no EIT effect), but only typical inverted OMIT spectrum. However, the on-resonance transparency window starts to appear upward between two side-

band dips at $J_1/J_2 = 0.5$ and then continues to increase this ratio, which will greatly amplify the coupled-cavity-induced EIT and hence the new sideband peaks occur at $J_1/J_2 = 1.6$. Finally, the spectrum implies a coupling effect of OMIT and EIT, that is, the CIT. Hence, the tunneling ratio can be deemed as the relative prominence of OMIT feature and EIT feature in the spectrum.

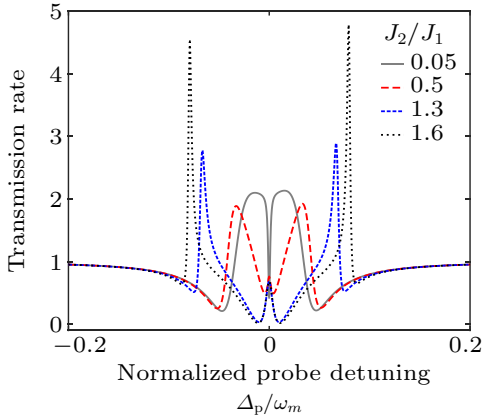



**Fig. 4.** Transmission spectra of probe light with different values of $J_1/J_2$. Other related parameters are $J_1 = \gamma_1$, $P_L = 1$ μW, and $\gamma_1 : \gamma_2 : \gamma_3 = 1 : -0.38 : 0.29$.

### 3.4. Effect of pump laser power ($P_L$) on the CIT spectrum

The pump laser power $P_L$ has an effect on the CIT spectrum. Under the condition of $\gamma_1 : \gamma_2 : \gamma_3 = 1 : -0.3 : 0.2$, $J_1 = \gamma_1$, and $J_1/J_2 = 1$, three cases of $P_L$ equal to 10, 100, and 300 μW are shown in Fig. 5. As for the on-resonance transparency window, it has a domical profile at $P_L = 100$ μW and 300 μW, but presents a spire-like lineshape at $P_L = 10$ μW. Besides, a larger pump laser power gently suppresses the two sideband peaks and thus increasing the width of the whole window, which corresponds with previous reports on OMIT features.

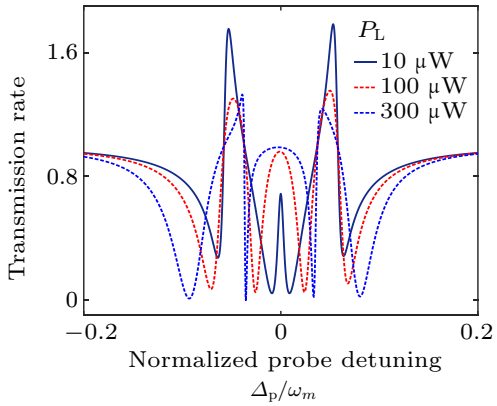



**Fig. 5.** Transmission spectra of probe light with different values of pump laser power ($P_L$). Other related parameters are $J_1 = \gamma_1$, $J_1/J_2 = 1$, and $\gamma_1 : \gamma_2 : \gamma_3 = 1 : -0.3 : 0.2$.

## 4. Slow and fast light

Slow light phenomenon and fast light phenomenon are closely associated with the induced transparency effect, and can be characterized by optical group delay given by

$$\tau_g = \left.\frac{d\mathrm{Arg}[t_p(\omega_p)]}{d\omega_p}\right|_{\omega_p=\omega_c}. \tag{9}$$

In contrast with the only slow light in a typical passive COM system, both highly tunable optical group delay and optically switching from slow to fast light are manifested in the proposed structure. Figure 6(a) shows the optical group delay as a function of pump power and optical gain (loss) rate $\gamma_2$, with three white dashed lines representing the following cross-section results in the three panels of Fig. 7(a), respectively. The gain–loss ratio of other two cavities is set to be $\gamma_1 : \gamma_3 = 1 : 0.6$. When the group delay has a value larger than zero, there exists the slow light phenomenon, and when the group delay is less than zero, there appears the fast light phenomenon.

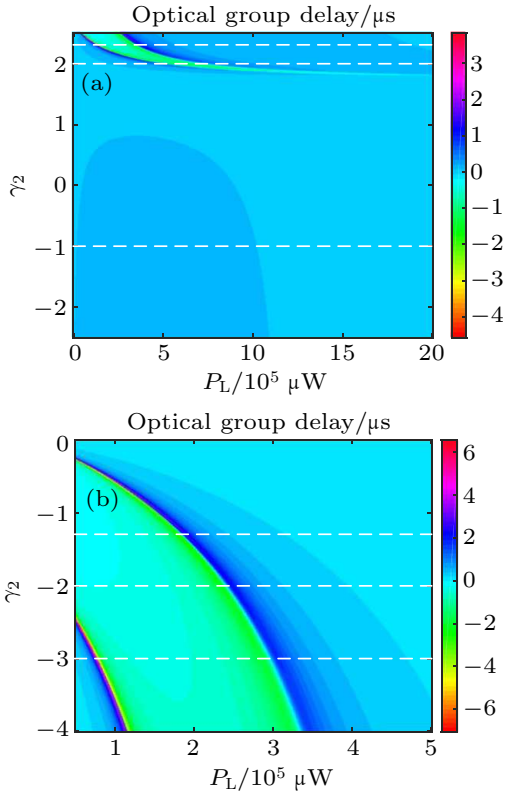



**Fig. 6.** Optical group delay *versus* pump power ($P_L$) and optical gain (loss) rate in the (a) second and (b) third resonators.

As for the three representative cases shown in Fig. 7(a), changing the power $P_L$ results in the fluctuation of group delay. At $\gamma_2 = 2.3\gamma_1$ in the upper panel, sharp fast–slow light transition is observed as the power increases. The middle panel exhibits a similar trend, but the transition is smoother. The group delay of CIT demonstrates the transition of slow-to-fast and fast-to-slow light, which are quite different from the common single transition phenomena.[8] However, at $\gamma_2 = -\gamma_1$, only time delay is present, indicating the slowing of light.

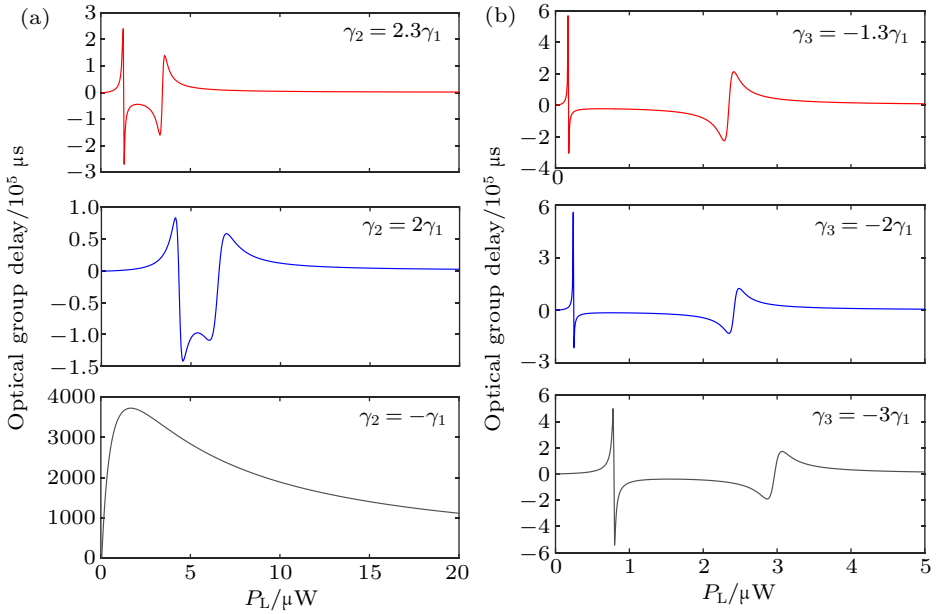



**Fig. 7.** Upper, middle, and bottom panels represent what are meant by white dashed lines in Figs. 6(a) and 6(b), respectively.

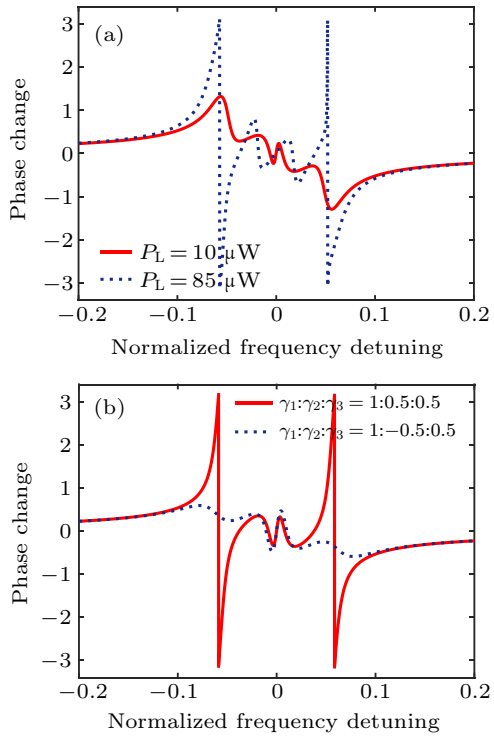



**Fig. 8.** (a) Plots of phase of the transmission amplitude varying with normalized frequency detuning at different values of (a) pump power ($P_L$) and (b) $\gamma_1 : \gamma_2 : \gamma_3$.

Figure 6(b) is for another condition and shows the optical group delay versus pump power and optical gain (loss) rate $\gamma_3$, and three white dashed lines which correspond to the cross-section results in the three panels of Fig. 7(b), respectively. The gain–loss ratio between other two cavities is set to be $\gamma_1 : \gamma_2 = 1 : 0.4$. Tunable group delay is clearly observed and the pump power threshold for achieving the fast–slow light transition can be modified via the optical gain (loss) rate $\gamma_3$ as indicated in the panels of Fig. 7(b). It is noteworthy that the CIT in this system can present two fast–slow light transitions (inter-transition) with pump power increasing monotonically, which is in contrast with the one- or two-cavity case, where only slow light[6] or one fast–slow light transition[8] is existent. Taking Fig. 7(b) for example, the group delay first experiences a sharp up-down peak and then a smooth down-up peak. This phenomenon can be understood as a combination of the effects caused by EIT and OMIT. The sharp pulse is greatly affected by $\gamma_3$, indicating its originality from EIT and the smooth pulse from OMIT. Also, the largest optical group delay is greatly enhanced to almost $6 \times 10^5$ μs. These results hold great potential for realizing the controllable switch from slow to fast light, which is useful in optical communication and signal processing.

In order to better illustrate the fast–slow light transition, figure 8 shows the calculated phases of the CIT transmission under different conditions. Figures 8(a) and 8(b) show the plots of phase change *versus* normalized frequency detuning at different values of pump power and $\gamma_1 : \gamma_2 : \gamma_3$, which greatly modify the evolution and sharpness of phase change.

## 5. Discussion

Although the CIT spectrum of the system is highly tunable, the basic guidelines can be given as follows. With the second cavity being an agent, the coupling of first (third) and second cavity results in an OMIT (EIT) feature. Therefore, the transmission characteristic is an interplay between OMIT and EIT. Changing the optical loss rate in the first (third) cavity mainly affects the OMIT (EIT) spectrum, that is, the on-resonance peak (two sideband peaks). An active second cavity will provide optical gain for both the OMIT and EIT, thus leading to an inverted spectrum. Tunneling ratio controls the relative prominence of OMIT feature and EIT feature in the

spectrum. The OMIT peak can widen with pump power increasing.

By adding a third cavity, the CIT effect can be realized in a compact COM structure, hence providing an insight into coupling phenomenon of two key types of induced transparency. The CIT spectrum can be employed to achieve highly controllable modulation of light propagation and enhance the sensing capability with its sharp transparency windows. Also, the optical group delay of CIT can present two pulses with the pump power increasing monotonically, indicating two slow-fast light switches. The advance or delay can be reached on a scale of hundreds of milliseconds.

## 6. Conclusions

In this paper, we propose a three-cavity compound COM structure with large tunable freedom and investigate the system's compound-induced transparency characteristics. The calculated CIT spectrum has distinctive features of multi-transparency windows and multi-sideband dips (peaks), which are collective effects of OMIT and EIT. Tunability of the CIT is demonstrated by evaluating the effects of spectrum-dominant parameters, namely the optical loss (gain) rate ($\gamma_2$, $\gamma_3$), the number and topology of active cavities, tunneling ratio ($J_1/J_2$), and pump laser power ($P_{\rm L}$). The optical group delay of CIT can reach hundreds of milliseconds. Notably, both fast-to-slow light switching and slow-to-fast light switching can be achieved by only monotonically increasing the pump power. This work presents a promising platform for further study on the compound-induced transparency features with advantageous tunability, controllable light propagation, fast–slow light switching, and engineering photons.

## References


[1] Liu Y C, Li B B and Xiao Y F 2017 *Nanophotonics* **6** 789
[2] Xiong H and Ying W 2018 *Appl. Phys. Rev.* **5** 031305
[3] Aspelmeyer M, Kippenberg T J and Marquardt F 2014 *Rev. Mod. Phys.* **86** 1391
[4] Peng B, Özdemir S K, Chen W, Nori F and Yang L 2017 *Nat. Commun.* **5** 5082
[5] Agarwal G S and Huang S 2010 *Phys. Rev. A* **81** 041803
[6] Safavi-Naeini A H, Mayer T P, Chan J, Eichenfield M, Winger M, Lin Q, Hill J T, Chang D E and Painter O 2011 *Nature* **472** 7341
[7] Weis S, Rivière R, Deléglise S, Gavartin E, Arcizet O, Schliesser A and Kippenberg T J 2010 *Science* **330** 1520
[8] Jing H, Özdemir S K, Geng Z, Zhang J, Lu X Y, Peng B, Yang L and Nori F 2015 *Sci. Rep.* **5** 9663
[9] Gu W J and Yi Z 2014 *Opt. Commun.* **333** 216
[10] Teufel J D, Li D, Allman M S, Cicak K, Sirois A J, Whittaker J D and Simmonds R W 2011 *Nature* **471** 204
[11] Rivière R, Deléglise S, Weis S, Gavartin E, Arcizet O, Schliesser A, Kippenberg T J 2011 *Phys. Rev. Lett.* **83** 063835
[12] Jiao Y, Lu H, Qian J, Li Y and Jing H 2016 *New J. Phys.* **18** 083034
[13] Jing H, Özdemir S K, Lu X Y, Zhang J, Yang L and Nori F 2014 *Phys. Rev. Lett.* **113** 053604
[14] Grudinin I S, Lee H, Painter O and Vahala K J 2010 *Phys. Rev. Lett.* **104** 083901
[15] Stannigel K, Komar P, Habraken S J M, Bennett S D, Lukin M D, Zoller P and Rabl P 2012 *Phys. Rev. Lett.* **109** 013603
[16] Kómár P, Bennett S D, Stannigel K, Habraken S J M, Rabl P, Zoller P and Lukin M D 2013 *Phys. Rev. A* **87** 013839
[17] Hill T J, Safavi-Naeini A H, Chan J and Painter O 2012 *Nat. Commun.* **3** 1196
[18] Fiore V, Yang Y, Kuzyk M C, Barbour R, Tian L and Wang H L 2011 *Phys. Rev. Lett.* **107** 133601
[19] Ludwig M, Safavi-Naeini A H, Painter O and Marquardt F 2012 *Phys. Rev. Lett.* **109** 063601
[20] Fan J and Zhu L 2012 *Opt. Express* **20** 20790
[21] Peng B, Özdemir S K, Lei F C, Monifi F, Gianfreda M, Long G L, Fan S H, Nori F, Bender C M and Yang L 2014 *Nat. Phys.* **10** 394
[22] Tohru O and Makoto T 2013 *Phys. Rev. A* **88** 013813